論文 / 著書情報
Article / Book Information

Title	Pre-training CNN for fast EUV lithography simulation including M3D effects
Authors	Hiroyoshi Tanabe, Akira Jinguji, Atsushi Takahashi
Citation	Proc. SPIE 12954, DTCO and Computational Patterning III, 129540I
Pub. date	2024, 4
DOI	https://doi.org/10.1117/12.3009880
Rights	(Copyright) Copyright 2024 Society of Photo-Optical Instrumentation Engineers (SPIE). One print or electronic copy may be made for personal use only. Systematic reproduction and distribution, duplication of any material in this publication for a fee or for commercial purposes, and modification of the contents of the publication are prohibited. (Citation) Hiroyoshi Tanabe, Akira Jinguji, and Atsushi Takahashi "Pre-training CNN for fast EUV lithography simulation including M3D effects", Proc. SPIE 12954, DTCO and Computational Patterning III, 129540I (10 April 2024); https://doi.org/10.1117/12.3009880

Pre-training CNN for fast EUV lithography simulation including M3D effects

Hiroyoshi Tanabe,* Akira Jinguji and Atsushi Takahashi
Tokyo Institute of Technology, 2-12-1 Ookayama, Meguro-ku, Tokyo 152-8550 Japan

ABSTRACT

Mask 3D (M3D) effects distort diffraction amplitudes from EUV masks. Electromagnetic (EM) simulations are used to rigorously calculate the distorted diffraction amplitudes. However, EM simulations are highly time consuming for OPC applications. The distorted diffraction amplitude can be characterized by M3D parameters. We develop a convolutional neural network (CNN) model which predicts M3D parameters very fast from input mask patterns. In this work, we train CNN using test mask data with various characteristics of metal layers. The accuracy of the CNN is good for the test mask data. However, when we use new mask data that mimic device patterns, the accuracy of the CNN is worsened. Starting from the CNN pre-trained by the test mask data, we improve the accuracy of the CNN by additional training using larger dataset including both the test mask data and the new mask data. The accuracy of the CNN is slightly improved by the fine tuning.

Keywords: lithography simulation, neural network, EUV mask

*tanabe.h.af@m.titech.ac.jp

1. INTRODUCTION

High aspect absorbers used in extreme ultraviolet (EUV) masks induce several mask 3D (M3D) effects such as critical dimension (CD) error and edge placement error.[1,2] It is necessary to include M3D effects in EUV lithography simulations. M3D effects are caused by the distorted diffraction amplitude from an EUV mask. The diffraction amplitude can be calculated rigorously by using electromagnetic (EM) simulators.[3-5] However, these calculations are highly time consuming, especially for optical proximity correction (OPC) applications.

To speed up the EM simulations, several models were proposed which approximate the rigorous domain decomposition method (DDM). Rigorous DDM[6] decomposes a mask pattern into many small patterns and calculates the EM amplitude iteratively to include the full order cross-talks between neighboring small patterns. In this way the non-locality of the EM interaction can be handled rigorously, but the computation is slow. On the other hand, approximate models[7-11] of DDM treat the EM interaction locally and include only low-order cross-talks between the neighboring patterns. The computation of these models is fast. However, high-order cross-talks become important for OPC masks due to the high pattern density. It could be difficult to apply these approximate models to OPC masks.

Recently, many models have been proposed, which apply convolutional neural network (CNN) to the EM simulation. In these models the non-locality of the EM interaction is fully included because the CNN connects all parts of the input mask pattern. These models are classified into three types depending on the target of CNN: near-field diffraction amplitude on the mask[12-15] or image intensity on the wafer[16,17] or far-field diffraction amplitude at the pupil.[18-21] In our model[18] six CNNs are used to predict the far-field diffraction amplitude from the input mask pattern. The image intensity on the wafer is calculated by applying Abbe's theory to the far-field diffraction amplitude.

In the previous paper[20] we constructed several CNNs for specific mask patterns. Ideally, CNN can be applied to arbitrary mask patterns. However, the accuracy of CNN depends on the quality and quantity of the training data. In this report we construct CNN for metal layers using a large dataset. We first generate one million test mask patterns including random L/S patterns, 14 nm vertical (V) and horizontal (H) lines. We train CNN using these test mask patterns and validate the accuracy. We also validate the accuracy of the CNN using new mask data that mimic device patterns. Typically, the accuracy of a CNN on new data is lower compared to the accuracy on original data. Starting from the CNN pre-trained by

DTCO and Computational Patterning III, edited by Neal V. Lafferty, Proc. of SPIE
Vol. 12954, 129540I · © 2024 SPIE · 0277-786X · doi: 10.1117/12.3009880

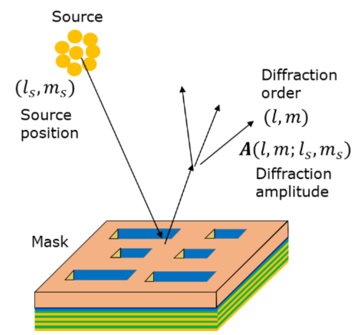

Fig. 1. Diffraction from an EUV mask.

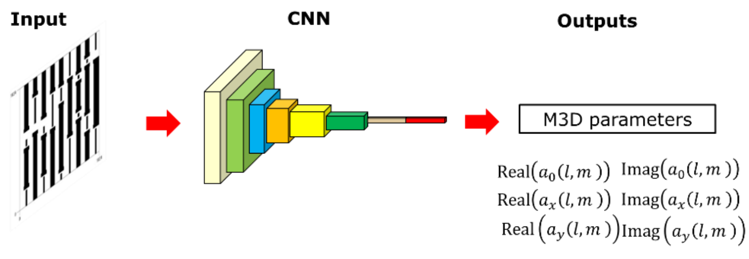

Fig. 2 CNN which predicts M3D parameters from a mask pattern.

the test mask data, we improve the accuracy of the CNN by additional training using larger dataset including both the test mask data and the new mask data.

In Sec. 2, we explain our CNN model. In Sec. 3, we train CNN by using one million test mask data. In Sec. 4, we fine-tune the CNN by adding 100 thousand new mask data to the training. Sec. 5 is the summary.

2. CNN FOR M3D PARAMETERS

In conventional optical lithography simulations, the light shielding film of a mask is assumed to be very thin. The far-field diffraction amplitude is calculated by the Fourier transformation (FT) of the mask pattern. The amplitude does not depend on the incident angle (or source position). However, in EUV lithography simulations, since the aspect ratio of the absorber is high, the far-field diffraction amplitude $\boldsymbol{A}(l, m; l_s, m_s)$ is calculated by the EM simulation. The amplitude depends on both the diffraction order (l, m) and the source position (l_s, m_s) (Fig. 1). Following our previous work,[18] we divide the thick mask diffraction amplitude $\boldsymbol{A}(l, m; l_s, m_s)$ into the thin mask amplitude $\boldsymbol{A}^{\mathrm{FT}}(l, m)$ (FT of the mask pattern) and the residual M3D amplitude $\boldsymbol{A}^{\mathrm{3D}}(l, m; l_s, m_s)$ as follows.

$$\boldsymbol{A}(l, m; l_s, m_s) = \boldsymbol{A}^{\mathrm{FT}}(l, m) + \boldsymbol{A}^{\mathrm{3D}}(l, m; l_s, m_s)\,. \tag{1}$$

The M3D amplitude for each diffraction order (l, m) smoothly depends on the source position (l_s, m_s). We approximate the M3D amplitude by a linear function of the source position as follows.

$$A_x^{\mathrm{3D}}(l, m; l_s, m_s) \cong a_0(l, m) + a_x(l, m)\,(l_s + l/2) + a_y(l, m)\,(m_s + m/2)\,, \tag{2}$$

where a_0 is the average of the amplitude and a_x and a_y are the slopes of the amplitude in x and y directions on the source plane, respectively. We call these three numbers as M3D parameters.

M3D parameters are determined by the mask pattern. We construct CNN which predict M3D parameters from an input mask pattern (Fig. 2). There are six CNNs depending on the targets: Real(a_0), Imag(a_0), Real(a_x), Imag(a_x), Real(a_y), and Imag(a_y). The accuracy of CNN depends on the training dataset. We examine the accuracy of CNN in the next sections.

3. PRE-TRAINING CNN BY BASIC DATASET

In this section we train CNN by using one million data (basic dataset). Figure 3 shows examples of mask patterns in the basic dataset. These are test patterns of metal layers. Type A, B, C, D, E include random L/S patterns, 14 nm V lines, 14 nm H lines, 14 nm V lines with OPC, 14 nm H lines with OPC, respectively. Both the bright field (BF) patterns and the dark field (DF) patterns are included. The size of the mask pattern is 512 nm X 512 nm on the wafer. We generate 2,000 original mask patterns for each mask type. Then we use the data augmentation technique[19] to increase the number of the data by a factor of 50. In the basic dataset there are 100 thousand data for each mask type and one million data in total.

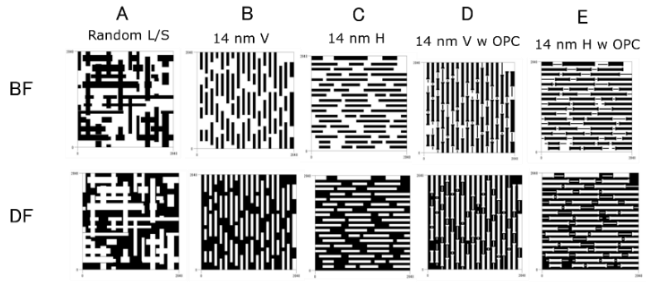

Fig. 3 Examples of the mask patterns included in the basic dataset.

Figure 4 shows the training and validation losses of six CNNs during the training. The number of targets for each CNN depend on the diffraction orders which pass the pupil of the projection optics. When the mask size is 512 nm X 512 nm, the number of the targets for Re(a_0) and Im(a_0) is 1,901 and the number of the targets for Re(a_x), Re(a_y), Im(a_x), Im(a_y) is 1,749. Both the training and validation losses become small after the training. The CNN successfully recognize the characteristics of metal layers.

Figure 5 shows the image intensities of a type A mask using EM simulation, FT, and CNN prediction. In the calculations we use NA 0.33, the wavelength λ 13.5 nm, and the dipole illumination DX90 σ 0.9/0.55 (X direction dipoles, open angle 90 degrees). The absorber material is Ta with 60 nm thickness. The difference between EM and CNN is much smaller than the difference between EM and FT. M3D effects of the mask are successfully reproduced by CNN.

Figure 6 shows the maximum intensity errors of type A~E mask patterns. The image intensity error of CNN is much smaller than that of FT. The difference between EM and FT is larger for horizontal patterns (C and E). This suggests larger M3D effects for horizontal patterns because the chief-ray of the incident light is tilted 6 degrees in Y direction.

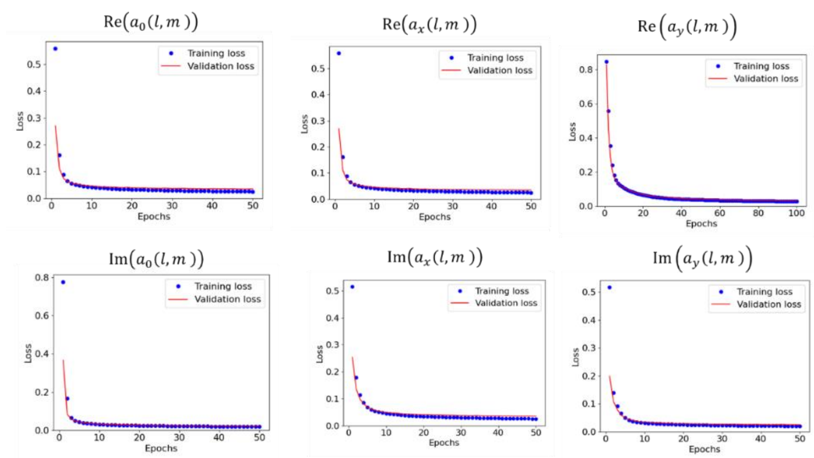

Fig. 4 Training and validation losses of CNNs for M3D parameters.

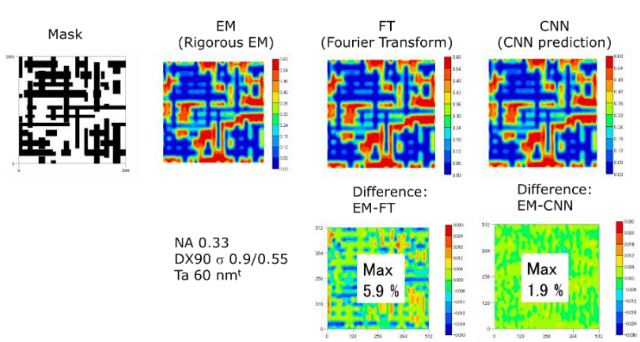

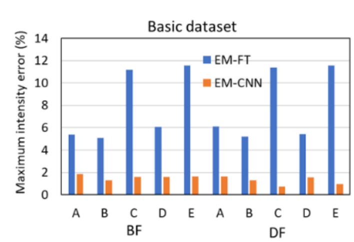

	Average error
EM-FT	7.9%
EM-CNN	1.4%

Fig. 5 Image intensities of EM, FT, and CNN models.

Fig. 6 Maximum intensity errors of mask patterns.

4. FINE TUNING CNN WITH NEW DATASET

In the previous section we constructed CNN that recognized the various test patterns of metal layers. In this section we evaluate the accuracy of the CNN using new mask data that mimic device patterns. Figure 7 is examples of the mask patterns included in the new dataset. We use 12 types of new mask patterns (A'~F', BF & DF).

First, we apply the CNN to this new dataset. Figure 8 shows the image intensities of a type A' mask. Lithography conditions are the same as in Fig. 5. We see that the difference between EM and CNN is small. The CNN successfully predict the M3D effects of the mask.

Figure 9 shows the maximum intensity errors of type A'~F' mask patterns. The image intensity error of CNN is much smaller than that of FT. The image intensities of CNN predictions are much better than those of the thin mask model. However, if we look more closely, the average image intensity error of CNN is 2.0%. The number is slightly larger than the value for the basic dataset, 1.4% in Fig. 6.

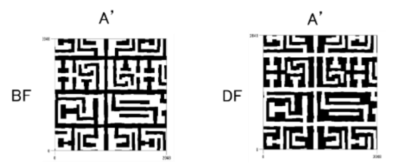

Fig. 7 Examples of mask patterns included in the new dataset.

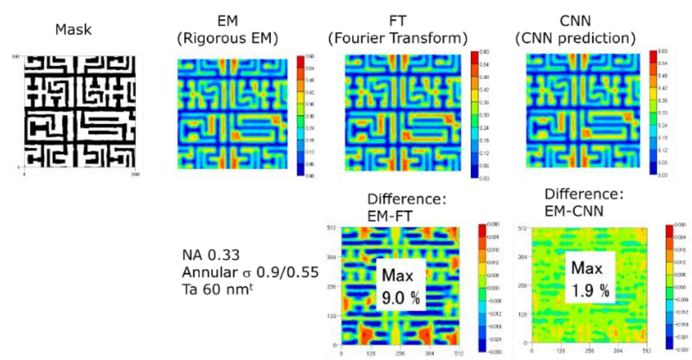

Fig. 8 Image intensities of EM, FT, and CNN models, and their differences.

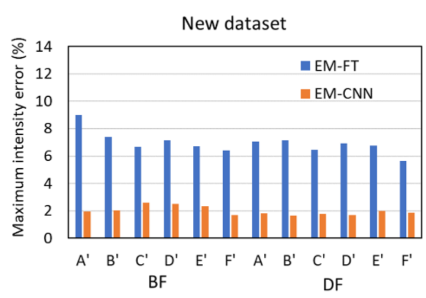

New dataset

	Average error
EM-FT	6.9%
EM-CNN	**2.0%**

Ref. Basic dataset

	Average error
EM-FT	7.9%
EM-CNN	**1.4%**

Fig. 9 Maximum intensity errors of type A'~F' mask patterns.

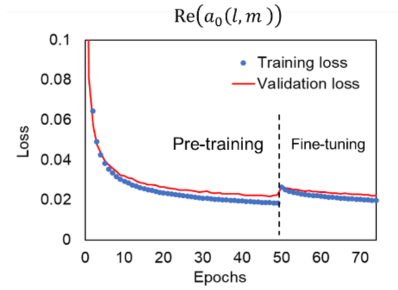

Fig. 10 Training and validation losses of pre-training and fine-tuning.

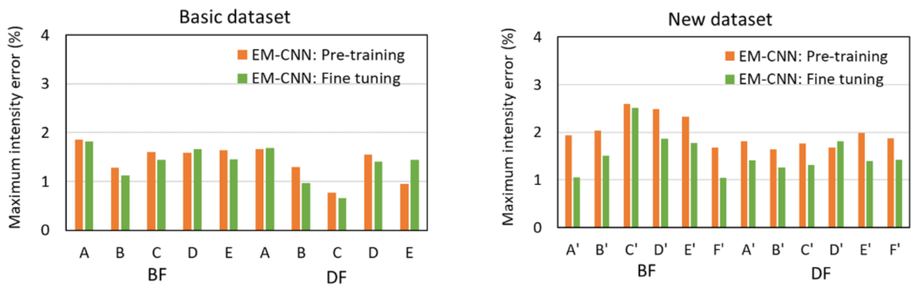

	Average error
EM-CNN: Pre-training	1.4%
EM-CNN: Fine-tuning	1.4%

	Average error
EM-CNN: Pre-training	2.0%
EM-CNN: Fine-tuning	1.8%

Fig. 11 Maximum intensity errors after pre-training and after fine-tuning.

In order to improve the accuracy, we fine-tune the CNN. The CNN constructed in Sec. 3 is used as the pre-trained CNN. We select 18 mask clips from each mask pattern (A'~F', BF & DF). The number of the original mask clips is 216. Data augmentation technique is used to increase the number of the data to 100 thousand. After the pre-training with one million basic data, we add 100 thousand new data for fine-tuning. In total 1.1 million data are used for fine-tuning. Figure 10 shows the training and validation losses of a M3D parameter a_0 during the pre-training (epochs 0~49) and the fine-tuning (epochs 50~74). The losses temporary increase after adding new data at epoch 50, but they decrease during the fine-tuning.

Figure 11 shows the results of the fine-tuning. The image intensity error of the basic dataset is almost unchanged after the fine-tuning. On the other hand, the image intensity error of the new dataset has been slightly reduced by the fine tuning. The average of the errors decreases from 2.0% to 1.8% by the fine-tuning.

5. SUMMARY

We trained CNN by using one million test mask data with various characteristic of metal layers. The targets of CNN are M3D parameters. The validation loss became very small after the training. The CNN successfully recognized the characteristics of metal layers. The image intensity error of CNN model was much smaller than that of FT.

The accuracy of the pre-trained CNN was validated using new mask data that mimicked device patterns. The accuracy was good, and the image intensity error of CNN model was much smaller than that of FT. Pre-trained CNN successfully predicted the M3D effects of the new masks.

However, when pre-trained CNN was applied, the image intensity error of the new dataset was slightly larger than that of the basic dataset. In order to reduce the image intensity errors, we fine-tuned the CNN. After the pre-training with one million basic data, we added 100 thousand new mask data for the fine-tuning. The fine tuning slightly reduced the image intensity error of the new dataset.

REFERENCES

[1] V. Philipsen, "Mask is key to unlock full EUV potential," Proc. SPIE 11609(2021).

[2] A. Erdmann, P. Evanschitzky, G. Bottiglieri, E. Setten and T. Fliervoet, "3D mask effects in high NA EUV imaging," Proc. SPIE 10957, 109570Z (2019).

[3] A. Wong and A. Neureuther, "Mask Topography Effects in Projection Printing of Phase-Shifting Masks," IEEE TRANSACTIONS ON ELECTRON DEVICES 41(1994)895.

[4] M.G. Moharam and T.K. Gaylord, "Rigorous coupled-wave analysis of planar-grating diffraction," J. Opt. Soc. Am. 71(1981)811.

[5] K.D. Lucas, H. Tanabe and A.J. Strojwas, "Efficient and rigorous three-dimensional model for optical lithography simulation," J. Opt. Soc. Am. A 13(1996)2187.

[6] L. Zschiedrich, S. Burger, A. Schaedle and F. Scmidt, "Rigorous finite-element domain decomposition method for electromagnetic near field simulations," SPIE 6924(2008)692450.

[7] K. Adam and A. R. Neureuther, "Simplified models for edge transitions in rigorous mask modeling," Proc. SPIE 4346(2001)331.

[8] A. Erdmann, C. Kalus, T. Schmoeller and A. Wolter, "Efficient simulation of light from 3-dimensional EUV-masks using field decomposition techniques," Proc. SPIE 5037(2003)482.

[9] P. Liu, Y. Cao, L. Chen, G. Chen, M. Feng, J. Jiang, H. Liu. S. Suh, S.W. Lee and S. Lee, "Fast and accurate 3D mask model for full-chip OPC and verification," Proc. SPIE 6520(2007)65200R.

[10] J. Word, C. Zuniga, M. Lam, M. Habib, K. Adam and M. Oliver, "OPC modeling and correction solutions for EUV lithography," Proc. SPIE 8166(2011)81660Q.

[11] V. Domnenko, B. Kuechler, W. Hoppe, J. Preuninger, U. Klostermann, W. Demmerle, M. Bohn, D. Krueger, R. Ryoung, H. Kim and L.E. Tan, "EUV computational lithography using accelerated topographic mask simulation," Proc. SPIE 10962(2019)169620O.

[12] S. Lan, J. Liu, Y. Wang, K. Zhao and J. Li, "Deep learning assisted fast mask optimization," Proc. SPIE 10587 (2018)105870H.

[13] P. Liu, "Mask synthesis using machine learning software and hardware platforms," Proc. SPIE 11327 (2020)1132707.

[14] R. Pearman, M. Meyer, J. Ungar, H. Yu, L. Pang and A. Fujimura, "Fast all-angle mask 3D ILT patterning," Proc. SPIE 11327(2020)113270F.

[15] J. Lin, L. Dong, T. Fan, X. Ma, R. Chen and Y. Wei, "Fast mask near-field calculation using fully convolution network," International Workshop Adv. Patterning Solutions (2020).

[16] W. Ye, M.B. Alawieh, Y. Watanabe, S. Nojima, Y. Lin and D.Z. Pan, "TEMPO: fast mask topography effect modeling with deep learning," Int. Symp. Phys. Design '20, (2020)127.

[17] A. Awad, P. Brendel, P. Evanschitzky, D.S. Woleamanual, A. Rosskopf and A. Erdmann, "Accurate prediction of EUV lithographic images and 3D mask effects using generative networks," J. Micro/Nanopattern. Mater. Metrol. 20(2021) 043201.

[18] H. Tanabe, S. Sato and A. Takahashi, "Fast EUV lithography simulation using convolutional neural network," J. Micro/Nanopattern. Mater. Metrol. 20(2021) 041202.

[19] H. Tanabe and A. Takahashi, "Data augmentation in extreme ultraviolet lithography simulation using convolutional neural network," J. Micro/Nanopattern. Mater. Metrol. 21(2022) 041602.

[20] H. Tanabe, A. Jinguji and A. Takahashi, "Evaluation of convolutional neural network for fast extreme violet lithography simulation using 3nm node mask patterns," J. Micro/Nanopattern. Mater. Metrol. 22(2023) 024201.

[21] H. Tanabe, A. Jinguji and A. Takahashi, "Accelerating extreme ultraviolet lithography simulation with weakly guiding approximation and source position dependent transmission cross coefficient formula," J. Micro/Nanopattern. Mater. Metrol. 23(2024) 014201.